Calibrating the marine turbidite paleoseismometer

Jamie D. Howarth[1], Alan R. Orpin[2], Yoshihiro Kaneko[3], Lorna J. Strachan[3], Scott D. Nodder[2], Joshu J. Mountjoy[2], Philip M. Barnes[2], Helen C. Bostock[2,5] and Caroline Holden[4]

[1]School of Geography, Environment and Earth Sciences, Victoria University of Wellington, PO Box 600, Wellington 6140, jamie.howarth@vuw.ac.nz

[2]National Institute of Water and Atmospheric Research (NIWA), Private Bag 14-901, Kilbirnie, Wellington 6241

[3]School of Environment, University of Auckland, Private Bag 92019, Auckland 1142

[4]GNS Science, PO Box 30-368, Lower Hutt 5040

[5]School of Earth and Environmental Sciences, University of Queensland, QLD 4066, Australia

Abstract

Subduction zones generate the largest and most damaging earthquakes and tsunami on Earth[1,2], but we do not fully understand the dynamics of these faults nor the hazard they poise due to the paucity of earthquake records that span millennia[1,3,4]. Arguably the most comprehensive subduction zone earthquake records have been produced using turbidite paleoseismology[5-12], an approach that reconstructs earthquake timing and magnitude from the geographic distribution of turbidite deposits formed by seismically triggered sediment flows[8-10,13,14]. Here we use observations of turbidites deposited by the 2016 M_w 7.8 Kaikōura earthquake in New Zealand to settle one of the most vigorous and unresolved debates in earthquake science: whether or not marine turbidites can be used to reconstruct the longest and most spatially complete subduction zone earthquake records[7,15-21]. The well-instrumented earthquake provides an ideal test for turbidite paleoseismology because for the first time the fault source, ground motions and turbidite deposition in discrete canyons are well-resolved. The Kaikōura earthquake triggered flows in eleven consecutive canyons along 200 km swath of the Hikurangi Subduction Margin (HSM) where a Peak Ground Velocity (PGV) exceeded a triggering threshold. The spatial distribution of turbidite deposition and their sedimentary structures validate the concepts used to reconstruct earthquake records from turbidites. We also show that the spatial distribution of turbidites may resolve the rupture directivity, which is an important breakthrough because it is essential for accurately quantifying ground motion hazard but is notoriously hard to define for prehistoric earthquakes. Furthermore, textural grading preserved within turbidites correlates with the velocity-time histories of earthquake ground motions, revealing a novel means to resolve the seismograms of pre-historic earthquakes. These new insights confirm that turbidites on active margins are sensitive natural seismometers that archive detailed information on earthquake occurrence, seismograms and rupture dynamics.

Introduction

Furthering our understanding of subduction zones dynamics and quantifying seismic and tsunami hazard requires paleoseismic records that span millennia because the return intervals for large earthquakes are commonly many hundreds to thousands of years[1,3,4]. Deep-sea turbidites can offer the longest and most spatially complete records of subduction zone earthquakes[8-10,13,14]. Despite a growing number of turbidite paleoseismology studies[5-10,22,23] vigorous debate persists[7,15-21] regarding the validity of the assumptions that underpin this method[13,24]. These are: (a) strong ground motions during earthquakes synchronously trigger turbidity currents along the length of ruptured subduction zones, eliminating localised triggers such as storm waves, floods or tides; and, (b) synchronicity can be established retrospectively from sedimentological and geochronological studies of sediment cores. With dating techniques currently limited (at best), by decadal uncertainties, turbidite paleoseismologists use two relative dating techniques to infer synchronicity – the 'confluence test' and 'turbidite fingerprinting.' Both approaches remain controversial due to the lack of direct observations from earthquake-triggered flows and their deposits[18,19,21]. A rigorous test of these hypotheses remains elusive because it requires detailed information on the fault rupture, the spatial distribution of strong ground motions produced by the earthquake, and spatially extensive sampling of coseismic turbidites. While previous studies have identified recently deposited turbidites triggered by earthquakes[8,25-27], datasets that meet all three criteria for testing turbidite paleoseismology have not previously existed. We use sediment cores from along the southern HSM, New Zealand, to identify turbidites triggered by the Kaikōura earthquake to provide the first rigorous test of turbidite paleoseismology methodologies.

Rupture geometry and slip distribution for the Kaikōura earthquake are well constrained by a combination of geodesy[28], seismology[29] and field-mapping[30] (Fig. 1A). The earthquake ruptured 21 onshore and offshore faults in a ~180-km long zone of the north eastern South Island. Such a well-constrained fault source facilitates physics-based models that are well corroborated by both near- and far-field station data[31], and show strong ground motions propagated along much of the southern HSM[31-33]. Post-earthquake sea floor mapping and sediment coring demonstrated that the earthquake caused widespread submarine landsliding, and triggered a turbidity current that travelled >680 km along the Hikurangi Channel (ref. [34]; Fig. 1A). The sedimentary distributary systems feeding the Hikurangi Channel are characterised by multiple feeder canyons that incise the continental shelf both parallel and perpendicular to the fault rupture, ideal for testing turbidite paleoseismology (Fig. 1B).

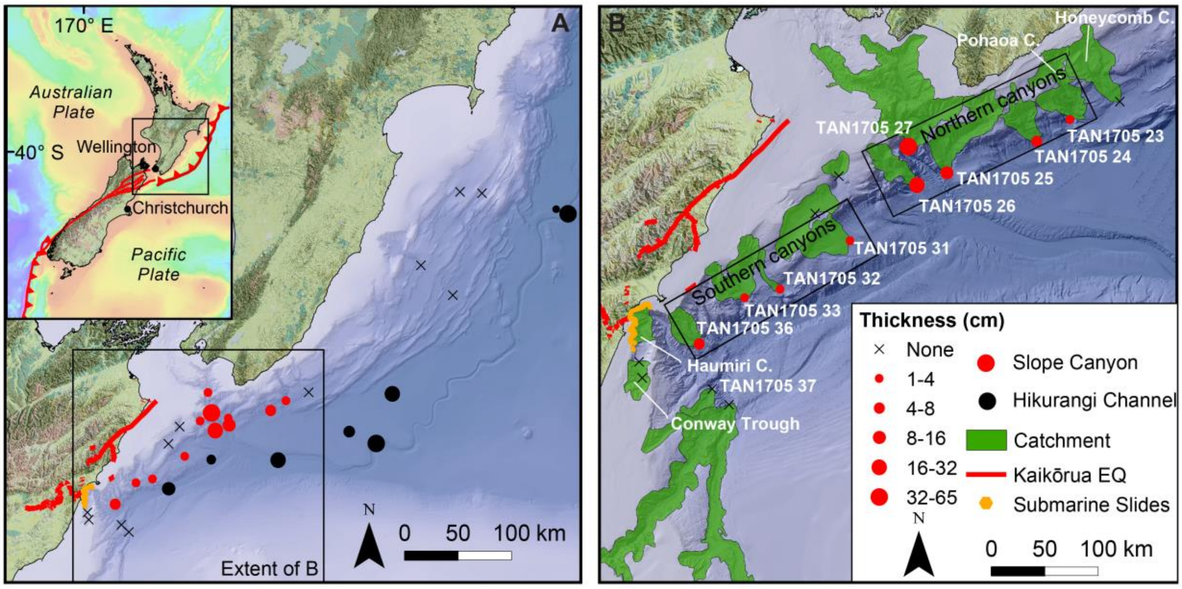

Figure 1: Tectonic setting and post-earthquake sample sites along the southern HSM. A) 2016 Kaikōura earthquake fault ruptures (red lines) and the spatial distribution, thickness of all coseismic turbidites (red dots) along the HSM and mapped submarine landslides (orange line)[34]. Inset: New Zealand's tectonic setting. B) Turbidite thickness and upstream catchment area (green polygons) for discrete sediment distributary systems, separated into southern and northern canyons.

Methods

Site selection and core sampling

Sediment samples were retrieved from the sea floor using a multicore corer designed to sample the sediment water interface and collecting cores up to 70 cm in length. Twenty core sites from along 700 km of the Hikurangi Subduction Margin (HSM) were selected using high-resolution digital elevation models (25 m grid) obtained from multi-beam bathymetry combined with backscatter and TOPAS PS18 sub-bottom acoustic profile data. Preliminary results from numerical modelling of turbidity currents in the software package Midland Valley Move were used to assess the likelihood that selected core sites could be impacted by canyon flushing flows large enough to overtop drainage divides in the Hikurangi sediment distributary system.

Cores were photographed and logged visually in the field and then analysed ashore using X-ray computed tomography (CT) conducted on a GE BrightSpeed medical CT scanner set to 120 kV, 250 mA, pitch of 0.625 mm and a 100 cm^2 window. CT tomography was processed in the software Imagej to produce sagittal slice images and down-core density curves at 625 micron resolution using the relationship of Reilly et al. (ref. [35]) for deriving bulk density from Hounsfield value/CT number. Cores were also linescan imaged and logged visually. High-resolution grainsize (~2.5 mm resolution) was conducted on the turbidites from selected cores using a Beckman Coulter LS 13 320 Multi-Wavelength Laser Diffraction Particle Size Analyser to establish the relationship between CT derived bulk density and mean grainsize. The geochemical composition of cores was characterised with micro-xrf core scanning using a COX analytical systems ITRAX XRF core scanner at a down core resolution of 1 mm.

Geochronology

Radiometric dating of turbidite sediments using the short-lived radioisotope ^{234}Th, which has a half-life of 24 days, provided quantitative evidence for recent emplacement. Once sediment is isolated from sea water through deposition, excess ^{234}Th activity becomes undetectable within 5 half-lives (120 days) of deposition. Consequently, the presence of excess ^{234}Th in the turbidite and the sediments that immediately underlie it provides evidence for very recent deposition. Radionuclide measurements were made on sediment from core TAN1613-53 from the Hikurangi Trough using gamma spectrometry at the Institute of Environmental Science and Research using a high-purity germanium detector. Activities are reported in $Bq.kg^{-1}$ and the uncertainties are based on the combined standard uncertainty multiplied by a coverage factor (k) = 2 (providing a level of confidence of 95%). Excess ^{234}Th was determined by repeat measurements where the initial samples where measured within three half-lives of the earthquake (72 days). Supported ^{234}Th was determined by re-measuring each sample after five half-lives (120 days) had elapsed. The reported excess ^{234}Th activities have been decay corrected to the dates of the earthquake.

The quantitative geochronology was used alongside CT tomography, high resolution imagery and geochemistry to develop qualitative indices of recent deposition from the TAN1613-53 core site. These indices include: 1) the presence of oxic sediments indicative of material recently at the sediment water interface located immediately below turbidites; 2) a lack of bioturbation in turbidites at core tops; 3) the presence of fresh biological remains in turbidite sediments; and where possible pre- and post-earthquake coring[34]. Oxic layers were identified visually and using downcore measurements of Fe/Mn ratios, which provides an indices for oxidation[36]. The degree of bioturbation was assessed using CT tomography to compare trace fossil abundance within the inferred Kaikōura turbidite with that in the underlying pre-earthquake sea floor sediment and in cores from other sites that lacked the Kaikōura turbidite at their core top. Repeat coring was also used to assess the degree of bioturbation that had occurred over the 8 months between the earthquake and the last coring campaign. Once established the qualitative indices of recent deposition were applied to identify the Kaikōura turbidite in the other cores from along the margin because their date of coring, 8 months after the earthquake, precluded the use of ^{234}Th dating.

Ground motion modelling

To simulate realistic Kaikōura earthquake waves, we use a source model of the earthquake developed previously[31] that fits local strong motion and geodetic (InSAR and GPS) data. We also follow the ground-motion simulation method as described in Holden et al.[31], in which synthetic ground motions are computed using open-source seismic wave propagation software SPECFEM3D[37,38]. This approach utilises 3D velocity and attenuation models for New Zealand[39] and topography and bathymetry of the region. The mesh spacing is 1 km on the Earth surface and gets coarser with depth. The topography and bathymetry are from STRM30 with the spatial resolution of 1-2 km. Numerical simulations are run on New Zealand's NeSI supercomputing cluster and the seismic waves are numerically accurate down to 2 seconds (0.5 Hz). With the smallest shear wave velocity of ~1 km.s^{-1} assumed in the current model set up, the smallest length scale of geological features influencing resulting ground motions is of the order of several kilometers, which are comparable or smaller than the sizes of the canyon catchments that produced turbidity currents. Synthetic ground-motion time series, expressed as the magnitude of three-component particle velocities $|v|$, and corresponding peak ground velocity (PGV) values are computed on a 4 km spaced grid covering on-shore and off-shore regions. We report PGV values rather than PGA which is usually used in marine paleoseismic studies because the PGV values have been validated against on-shore strong-motion and high-rate GPS data along the entire Hikurangi margin[31].

The assumed 3D velocity model indicates the presence of the low-velocity sedimentary wedge of the outer forearc (Fig. S6), although the resolution of the tomographic model offshore is relatively low. The presence of such a low-velocity zone amplifies the resulting ground motions via basin-directivity coupling[32], which may enhance the triggering of sub-marine landslides. To assess the effect of the uncertainty in off-shore velocity model on the simulated ground motions at turbidite sources/underwater canyons, we compute synthetic ground motions using a 1D, layered velocity model (Fig. S5). The 1D velocity model was derived from the spatial average of seismic velocities (Vp and Vs), densities and anelastic attenuations (Qp and Qs) at different depth slices in the 3D velocity model.

Including the assumed 3D shear wave velocity model in the ground motion simulation results in a band of high PGV extending from the northern tip of the Kaikōura fault rupture, ~300 km along the upper continental slope of the outer forearc. In this model PGVs are elevated above those produced by the 1D model in the area of turbidity current triggering by a factor of 2 on average (Fig. S5). Both models produce consistent threshold relationships between triggering and no triggering of turbidity currents but the threshold PGV for the 3D simulation is ~17 $cm.s^{-1}$ compared to just ~8 $cm.s^{-1}$ for the 1D equivilent. We adopt the 3D simulation as the prefered model because the PGVs produced by it show better fit to the observed station data than those from the 1D model (Fig. S4).

Coseismic turbidite structure and spatial distribution

The spatial distribution of turbidite deposition resulting from the 2016 Kaikōura earthquake was determined using sediment cores collected during two campaigns that occurred three days (voyage TAN1613) and 8 months (TAN1705) after the earthquake. Twenty discrete canyon or slope-basin catchments were sampled, along 700 km of the southern and central HSM (Fig. 1A). The presence/absence of new turbidites was determined using a combination of short-lived radioisotope dating (^{234}Th) and lithological indicators of recent deposition (such as lack of bioturbation, an underlying oxic layer indicative of recent seafloor surficial sediments, and freshly buried biological remains[34]; Fig. 2; Fig. S1; Supplementary information).

Coseismic turbidites have an average thickness of ~100 mm but are highly variable (20–650 mm, Fig. 2). While sedimentary structures of the turbidites, and their inferred emplacement flow characteristics, vary between canyons and with distance down-channel from source areas (Supplementary information; Fig. 2), there is remarkable coherence in the number of normally graded grainsize pulses. Here, we define a grainsize pulse as a discrete, normally graded interval, generally characterised by planar laminated very-fine sandy silts (T_D) overlain by normally graded mud (T_{E-1} or T_{E-2}) (cf. ref. [40-42]). These grainsize pulses are also resolved in core imagery and high-resolution down-core density profiles produced by CT tomography, which provide a verified proxy for mean grainsize (Fig. S2). In southern canyons adjacent to the fault rupture the turbidites are characterised by a single grainsize pulse (Fig. 2; Supplementary information). In contrast, turbidites in northern canyons, northeast of the rupture tip, are much more complex and contain three distinct graded pulses (Supplementary information). The number of grainsize pluses is coherent across canyons within each zone despite the differences in distance from source, number of channel confluences upstream of the deposit and sediment-source areas (Fig. 2).

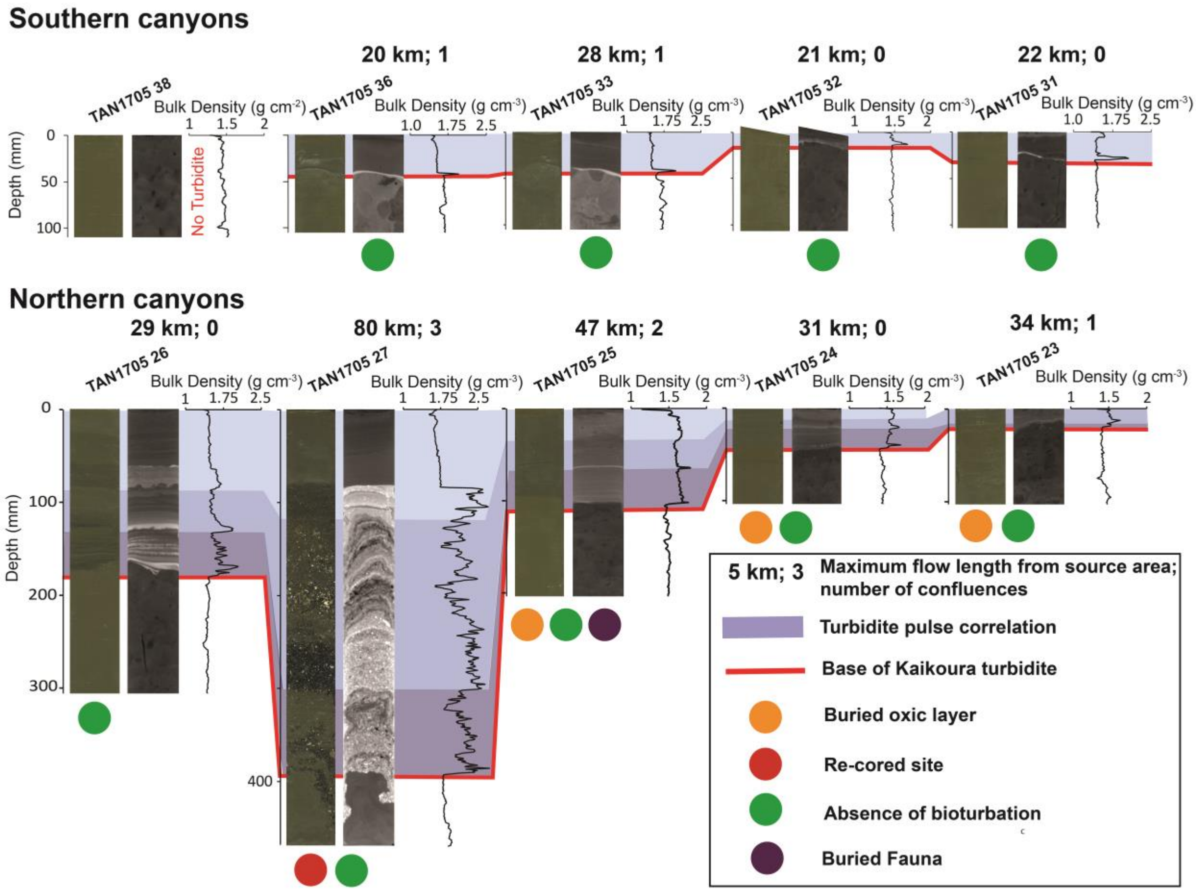

Figure 2: Coherence of Kaikōura earthquake turbidites from the southern and northern canyons. Core image, CT tomography scans and plots of bulk density are shown. The number of grainsize pulses recorded by down-core density profiles correlates across turbidites within the southern (n=1) and northern (n=3) canyons (see Figure 1 for the locations).

Triggering of turbidity currents by the Kaikōura earthquake was identified over a >200 km length of the margin in 11 consecutive canyons (Fig. 3A). The NE and SW extents of triggering exist both 120 km north of the rupture tip between the Pahaoa and Honeycomb canyons and 15 km SE of the southern extent of rupture in the Conway Trough (Fig. 3A). Turbidity-current triggering is interrupted along strike only by the absence of recent turbidites in cores from the upper Marlborough slope basin (Fig. 3A). An explanation for this absence could be the older age and greater consolidation of the sediment exposed in the head of the gully that supplies sediment to the basin (Fig. S3). There, sea-floor samples and sediment thicknesses estimated from sub-bottom profiles reveal mid Pleistocene or older units outcropping at the seafloor[43], and little or no post-glacial (<20 ka) deposition on the outermost shelf. We infer that these characteristics make this locality less sensitive to seismic shaking and less likely to trigger a turbidity current than other locations along the margin, and therefore, do not consider it further in our analysis of the relationship between strong ground motions and turbidite emplacement.

Correlating ground motions with coseismic turbidites

To qualify the relationship between the spatial pattern of landslide triggering, turbidite deposition, and shaking from the Kaikōura earthquake, we perform a physics-based ground-motion simulation of the earthquake. Simulations are based on a published fault source model[31] and an approach that accounts for both 3D velocity and attenuation models for New Zealand (Methods). Modelled ground motions are expressed in terms of the magnitude of surface ground velocity calculated up to 0.5 Hz and are validated against on-shore seismic and geodetic data along the length of the HSM (ref. [32]; Fig. S4). Modelled PGV's are highest in close proximity to the rupture and NE of the rupture tip due to the directivity and amplification of motions in the low-velocity sedimentary prism of the subduction zone[32]. We find that the radiating pattern of seismic energy along the rupture and northwards of its tip is well reflected by the finite pattern of turbidity current triggering in canyons (Fig. 3A); the first time such a comparison has been achieved. Turbidites were deposited in distributary systems that experienced PGV's in excess of 17 $cm.s^{-1}$ (Fig. 3A). The specific PGV threshold depends on the assumed velocity model, but this spatial pattern of PGV's is retained in simulations with different velocity models (Fig. S5).

Remarkably, velocity-time histories from the Kaikōura earthquake recorded by the strong ground motion stations nearest the southern (site KIKS) and northern (site NTWS) canyons show the same number of prominent amplitude peaks (defined here as > 50% of the maximum amplitude) as there are normally graded grainsize pulses in turbidites from these zones (Fig. 3B). A single velocity-amplitude peak correlates with a single grainsize pulse in turbidites from the southern canyons, while three peaks correlate with three pulses in turbidites from the northern canyons (Fig. 3B). Despite this compelling agreement, no direct quantitative comparisons are possible due to the spatial separation between the recording stations and the canyon catchments that produced turbidity currents. To explore this relationship between earthquake seismograms and turbidite structure further we use the ground motion simulation to extract the velocity-time history of the earthquake for the centroid of each canyon catchment. Using the turbidity current triggering threshold of >17 $cm.s^{-1}$, the number of velocity amplitude peaks above this threshold show coherence with the number of normally-graded grainsize pulses within the coseismic turbidite (Fig. 3C). Modelled PGV–amplitude peaks above the triggering threshold also replicate the observed difference in the number of amplitude peaks and grainsize pulses between the southern and northern canyons (Fig. 3C).

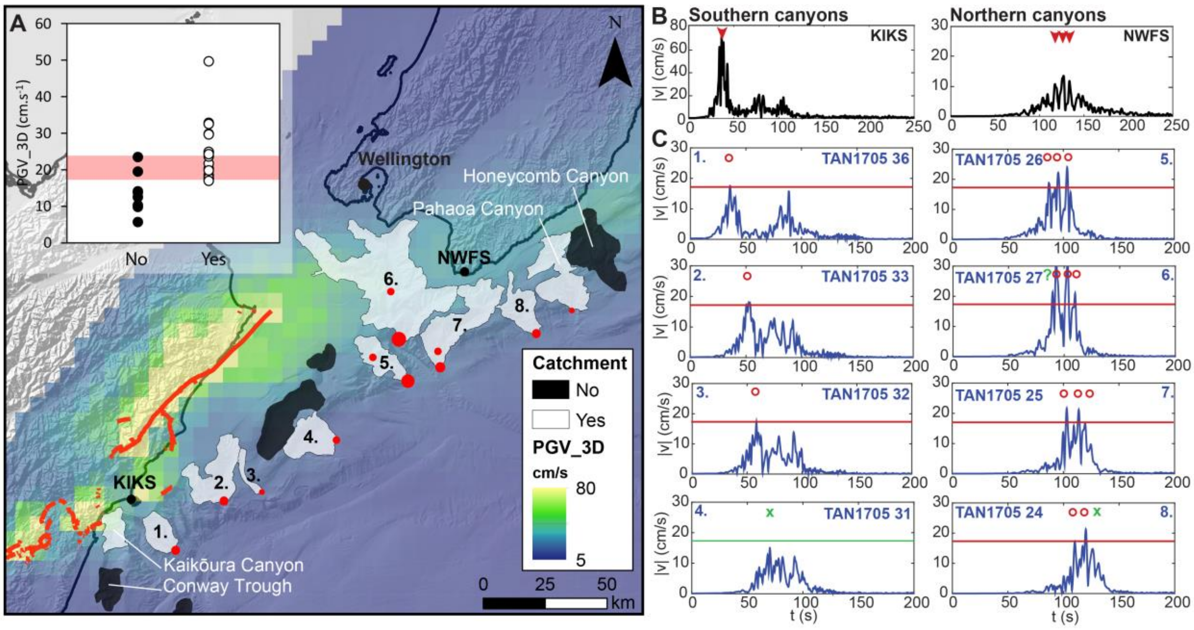

Figure 3: The relationship between fault source, ground motions and turbidite deposition. A) The spatial distribution of peak ground velocity (PGV) and turbidite deposition. Inset: Populations of PGVs for landslide triggering (Yes) and no triggering (No) used to derive the triggering threshold. **B)** The closest strong motion stations to the southern and northern canyons (KIKS and NWFS stations, respectively) show the same number of prominent amplitude peaks in the magnitude of PGV's |v| (black) as there are turbidite grainsize pulses in these zones (red arrows). **C)** Comparison between the number of amplitude peaks in synthetic velocity-time histories (blue) above the triggering threshold (17 $cm.s^{-1}$) and grainsize pulses in turbidites from the southern and northern canyons. Horizontal coloured lines – triggering threshold exceeded (red) or not exceeded (green) by amplitude peaks. Red circles – normally graded grainsize pulses that correspond to amplitude peaks; Green crosses (TAN1705-24, TAN1705-31) – grainsize pulse with no corresponding amplitude peak exceeding the defined threshold. Green question mark (TAN1705-27) – amplitude peak with no corresponding grainsize pulse.

Validation of turbidite paleoseismology

The observation that the spatial distribution of coseismic turbidites correlates with ground motions modelled from a well-constrained fault source supports the hypothesis that synchronous triggering of turbidity currents along subduction margins record earthquakes. Hence, deposition of coseismic turbidites provides a sensitive natural archive for reconstructing the frequency (if not the precise source) of past large earthquakes. However, the effectiveness of such an approach for paleoseismological purposes requires that the spatial distributions of earthquake-triggered turbidites be reliably identified over millennia in the sedimentary record.

Synchronous deposition of turbidites in the sedimentary record is established using two relative dating techniques, the 'confluence test' and 'turbidite finger printing' because numerical dating techniques have statistical uncertainties that span decades[18,19,21]. The confluence test uses the number of turbidites between temporal datums above and below the confluence of major submarine channels/canyons[13,14,44]. The idea is that flows triggered synchronously in separate canyon heads will produce a single turbidite above and below the confluence of the canyons. In contrast, asynchronous flows will produce one deposit above and two below the confluence. Analysis of the number of turbidites emplaced following the Kaikōura earthquake shows a single deposit above and below all canyon and channel confluences, across channel thalweg scales of tens to hundreds of kilometres (Fig. S3). This observation demonstrates the utility of the confluence test for establishing synchronous deposition from sedimentary records of turbidites.

Turbidite 'finger printing' has been used to make arguments of synchronicity in locations where it is not possible to use the confluence test[7,8,40], based on the observation that turbidites with the same numerical age distributions from different canyons have similar patterns of grainsize pulsing. Correlation of these so called 'multi-pulsed turbidites' have been proposed for discrete canyons separated by along margin distances of up to 1000 km, and imply that separate flows share the same number of velocity pulses, each relating to an episode of canyon head mass-wasting[14]. Proponents of this approach argue that a common ground motion-time history from a large earthquake is the only process capable of causing simultaneous triggering of multiple phases of canyon head mass-wasting, and in turn velocity pulses in turbidity currents over such large distances[8,14,45]. The preservation of discrete velocity pulses in flows driven by different phases of mass-wasting has recently been validated in flume simulations[46]. Detailed analysis of Kaikōura turbidite stratigraphy herein demonstrates that the ground motion-time history of the triggering earthquake is an underpinning process controlling the fidelity of grainsize pulses in turbidites deposited in adjacent but discrete distributary systems. Further, there is coherence in the number of turbidite grainsize pulses and the number of ground motion peaks above threshold amplitudes required to trigger turbidity currents. This observation supports the turbidite 'finger printing' hypothesis in natural systems despite complexity, such as variable thalweg lengths and the number of upstream confluences.

Discussion

The Kaikōura earthquake case study provides the first comprehensive evidence from an observed earthquake that validates a range of assumptions that underpin turbidite paleoseismology[18,19,21]. However, the observed relationships between the fault source, rupture directivity, ground motions and the spatial distribution of coseismic turbidites, raise some important issues and opportunities. This study illustrates that not all coseismic turbidites on subduction margins owe their origin to plate interface ruptures, emphasising the need to evaluate all potential earthquake sources in regional paleoseismic investigations[47-49]. Our study also demonstrates that using the spatial distribution of turbidites as a proxy for rupture length and earthquake magnitude is complicated by the asymmetric radiation of ground motions from a specific fault source. This asymmetry is caused by a combination of rupture directivity, and the radiating patterns and amplification of earthquake ground motions in low velocity sedimentary prisms[32]; physical attributes that are common on subduction zones globally. Rather than being a limitation, the nuanced relationship between fault rupture, the spatial distribution of ground motions and turbidite triggering offers the potential to resolve earthquake rupture directivity in paleoseismic events constrained by additional proxies, such as rupture length from coastal vertical deformation paleoseismology. The potential of coseismic turbidites to provide a proxy for rupture directivity is an important breakthrough as directivity is essential for accurately quantifying ground-motion hazard[50] but is notoriously hard to define for prehistoric earthquakes[51,52].

The pattern of grainsize pulses observed in the Kaikōura coseismic turbidites described herein highlights the challenge of using turbidite fingerprinting alone to demonstrate synchronous deposition. Until now, such dual fingerprints (i.e., northern versus southern canyons) would likely have been interpreted as two separate earthquakes if reconstructed from the sediment record alone. Our study demonstrates that if synchronous turbidite deposition can be established independently using the confluence test then turbidite fingerprinting may provide an unprecedented level of information on the rupture dynamics of prehistoric earthquakes. It is plausible then, to view co-seismic turbidites as natural seismometers, which archive detailed information on the seismograms of pre-historic earthquakes. Such information may advance our ability to identify asperities on subduction zone faults, estimate earthquake magnitude and quantify spatial variation in ground motions using turbidite records[53]. Finally, now that the underpinning hypotheses of turbidite paleoseismolgy have been validated, turbidite histories must be regarded as fundamental for understanding the dynamics of subductions zones and quantification of their potential hazard[12,14,26,54]

Acknowledgement

Funding for core analysis was provided by an EQC biennial research grant (No 18/756) awarded to JDH, ARO and SDN. Voyages in 2016 and 2017 were funded by Ministry of Business, Innovation and Employment (MBIE) Tangaroa Reference group and the MBIE Endeavour Fund research programme 'Hikurangi subduction earthquakes and slip behaviour'. NIWA scientists were co-funded by a MBIE Strategic Science Investment Fund in the Physical Resources programme in NIWA's Coasts and Oceans Centre. YK was funded by a Rutherford Foundation Discovery Fellowship.

Author contributions

JDH designed the study with input from ARO and YK. PMB, JDH and JJD identified cores sites. JDH, ARO, SDN and PMB undertook the field sampling. JDH, ARO, LJS, HCB, SDN generated and interpreted the core sedimentological and geochemical data. YK and CH conducted the ground motion modelling. JDH and ARO wrote the paper with input from all co-authors.

References

1 Simons, M. *et al.* The 2011 Magnitude 9.0 Tohoku-Oki Earthquake: Mosaicking the Megathrust from Seconds to Centuries. *Science* **332**, 1421-1425, doi:10.1126/science.1206731 (2011).

2 Bilek, S. L. & Lay, T. Subduction zone megathrust earthquakes. *Geosphere* **14**, 1468-1500, doi:10.1130/GES01608.1 (2018).

3 Normile, D. Scientific Consensus on Great Quake Came Too Late. *Science* **332**, 22-23, doi:10.1126/science.332.6025.22 (2011).

4 Sieh, K. *et al.* Earthquake Supercycles Inferred from Sea-Level Changes Recorded in the Corals of West Sumatra. *Science* **322**, 1674-1678, doi:10.1126/science.1163589 (2008).

5 Goldfinger, C. *et al.* Late Holocene rupture of the northern San Andreas fault and possible stress linkage to the Cascadia subduction zone. *Bulletin of the Seismological Society of America* **98**, 861-889, doi:10.1785/0120060411 (2008).

6 Gracia, E. *et al.* Holocene earthquake record offshore Portugal (SW Iberia): testing turbidite paleoseismology in a slow-convergence margin. *Quaternary Science Reviews* **29**, 1156-1172, doi:10.1016/j.quascirev.2010.01.010 (2010).

7 Goldfinger, C. *et al.* The importance of site selection, sediment supply, and hydrodynamics: A case study of submarine paleoseismology on the northern Cascadia margin, Washington USA. *Marine Geology* **384**, 4-46, doi:10.1016/j.margeo.2016.06.008 (2017).

8 Patton, J. R. *et al.* A 6600 year earthquake history in the region of the 2004 Sumatra-Andaman subduction zone earthquake. *Geosphere* **11**, 2067-2129, doi:10.1130/ges01066.1 (2015).

9 Moernaut, J. *et al.* Larger earthquakes recur more periodically: New insights in the megathrust earthquake cycle from lacustrine turbidite records in south-central Chile. *Earth and Planetary Science Letters* **481**, 9-19, doi:https://doi.org/10.1016/j.epsl.2017.10.016 (2018).

10 Moernaut, J. *et al.* Lacustrine turbidites as a tool for quantitative earthquake reconstruction: New evidence for a variable rupture mode in south central Chile. *Journal of Geophysical Research-Solid Earth* **119**, 1607-1633, doi:10.1002/2013jb010738 (2014).
11 Usami, K., Ikehara, K., Kanamatsu, T. & McHugh, C. M. Supercycle in great earthquake recurrence along the Japan Trench over the last 4000 years. *Geoscience Letters* **5**, 11, doi:10.1186/s40562-018-0110-2 (2018).
12 Goldfinger, C., Ikeda, Y., Yeats, R. S. & Ren, J. J. Superquakes and Supercycles. *Seismological Research Letters* **84**, 24-32, doi:10.1785/0220110135 (2013).
13 Goldfinger, C. in *Annual Review of Marine Science, Vol 3* Vol. 3 *Annual Review of Marine Science* (eds C. A. Carlson & S. J. Giovannoni) 35-66 (2011).
14 Goldfinger, C. *et al.* Turbidite event history—Methods and implications for Holocene paleoseismicity of the Cascadia subduction zone. *U.S. Geological Survey Professional Paper* **1661–F**, 170 p. (2012).
15 Goldfinger, C. *et al.* Can turbidites be used to reconstruct a paleoearthquake record for the central Sumatran margin?: COMMENT. *Geology* **42**, e344-e344, doi:10.1130/G35558C.1 (2014).
16 Goldfinger, C., Wong, I., Kulkarni, R. & Beeson, J. W. Reply to "Comment on 'Statistical Analyses of Great Earthquake Recurrence along the Cascadia Subduction Zone' by Ram Kulkarni, Ivan Wong, Judith Zachariasen, Chris Goldfinger, and Martin Lawrence" by Allan Goddard Lindh. *Bulletin of the Seismological Society of America* **106**, 2935-2944, doi:10.1785/0120150282 (2016).
17 Lindh, A. G. Comment on "Statistical Analyses of Great Earthquake Recurrence along the Cascadia Subduction Zone" by Ram Kulkarni, Ivan Wong, Judith Zachariasen, Chris Goldfinger, and Martin Lawrence. *Bulletin of the Seismological Society of America* **106**, 2927-2934, doi:10.1785/0120150069 (2016).
18 Shanmugam, G. Comment on "Late Holocene Rupture of the Northern San Andreas Fault and Possible Stress Linkage to the Cascadia Subduction Zone" by Chris Goldfinger, Kelly Grijalva, Roland Bürgmann, Ann E. Morey, Joel E. Johnson, C. Hans Nelson, Julia Gutiérrez-Pastor, Andrew Ericsson, Eugene Karabanov, Jason D. Chaytor, Jason Patton, and Eulàlia Gràcia. *Bulletin of the Seismological Society of America* **99**, 2594-2598, doi:10.1785/0120080030 (2009).
19 Sumner, E. J. *et al.* Can turbidites be used to reconstruct a paleoearthquake record for the central Sumatran margin? *Geology* **41**, 763-766, doi:10.1130/g34298.1 (2013).
20 Talling, P. J. *et al.* KEY FUTURE DIRECTIONS FOR RESEARCH ON TURBIDITY CURRENTS AND THEIR DEPOSITS. *Journal of Sedimentary Research* **85**, 153-169, doi:10.2110/jsr.2015.03 (2015).
21 Atwater, B. F., Carson, B., Griggs, G. B., Johnson, H. P. & Salmi, M. Rethinking turbidite paleoseismology along the Cascadia subduction zone. *Geology* **42**, 827-830, doi:10.1130/G35902.1 (2014).
22 Howarth, J. D., Fitzsimons, S. J., Norris, R. J. & Jacobsen, G. E. Lake sediments record high intensity shaking that provides insight into the location and rupture length of large earthquakes on the Alpine Fault, New Zealand. *Earth and Planetary Science Letters* **403**, 340-351, doi:10.1016/j.epsl.2014.07.008 (2014).
23 Howarth, J. D., Fitzsimons, S. J., Norris, R. J., Langridge, R. & Vandergoes, M. J. A 2000 yr rupture history for the Alpine fault derived from Lake Ellery, South Island, New Zealand. *Geological Society of America Bulletin* **128**, 627-643, doi:10.1130/b31300.1 (2016).
24 Goldfinger, C. in *International Geophysics* Vol. 95 119-170 (Academic Press, 2009).
25 McHugh, C. M. *et al.* Offshore sedimentary effects of the 12 January 2010 Haiti earthquake. *Geology* **39**, 723-726, doi:10.1130/g31815.1 (2011).

26 Ikehara, K. *et al.* Documenting large earthquakes similar to the 2011 Tohoku-oki earthquake from sediments deposited in the Japan Trench over the past 1500 years. *Earth and Planetary Science Letters* **445**, 48-56, doi:https://doi.org/10.1016/j.epsl.2016.04.009 (2016).
27 Van Daele, M. *et al.* A comparison of the sedimentary records of the 1960 and 2010 great Chilean earthquakes in 17 lakes: Implications for quantitative lacustrine palaeoseismology. *Sedimentology* **62**, 1466-1496, doi:10.1111/sed.12193 (2015).
28 Hamling, I. J. *et al.* Complex multifault rupture during the 2016 M_w 7.8 Kaikōura earthquake, New Zealand. *Science* **356**, doi:10.1126/science.aam7194 (2017).
29 Kaiser, A. *et al.* The 2016 Kaikōura, New Zealand, Earthquake: Preliminary Seismological Report. *Seismological Research Letters* **88**, 727-739, doi:10.1785/0220170018 (2017).
30 Litchfield, N. J. *et al.* Surface Rupture of Multiple Crustal Faults in the 2016 Mw 7.8 Kaikōura, New Zealand, Earthquake. *Bulletin of the Seismological Society of America* **108**, 1496-1520, doi:10.1785/0120170300 (2018).
31 Holden, C. *et al.* The 2016 Kaikoura Earthquake Revealed by Kinematic Source Inversion and Seismic Wavefield Simulations: Slow Rupture Propagation on a Geometrically Complex Crustal Fault Network. *Geophysical Research Letters* **44**, 11320-11328, doi:10.1002/2017gl075301 (2017).
32 Wallace, L. M. *et al.* Large-scale dynamic triggering of shallow slow slip enhanced by overlying sedimentary wedge. *Nature Geoscience* **10**, 765-+, doi:10.1038/ngeo3021 (2017).
33 Bradley, B. A., Razafindrakoto, H. N. T. & Polak, V. Ground-Motion Observations from the 14 November 2016 M-w 7.8 Kaikoura, New Zealand, Earthquake and Insights from Broadband Simulations. *Seismological Research Letters* **88**, 740-756, doi:10.1785/0220160225 (2017).
34 Mountjoy, J. J. *et al.* Earthquakes drive large-scale submarine canyon development and sediment supply to deep-ocean basins. *Science Advances* **4**, doi:10.1126/sciadv.aar3748 (2018).
35 Reilly, B. T., Stoner, J. S. & Wiest, J. SedCT: MATLAB™ tools for standardized and quantitative processing of sediment core computed tomography (CT) data collected using a medical CT scanner. *Geochemistry, Geophysics, Geosystems*, n/a-n/a, doi:10.1002/2017GC006884.
36 Rothwell, R. G. & Croudace, I. w. in *Micro-XRF Studies of Sediment Cores: Applications of a non-destructive tool for the environmental sciences* (eds Ian W. Croudace & R. Guy Rothwell) 25-102 (Springer Netherlands, 2015).
37 Komatitsch, D. & Tromp, J. Introduction to the spectral element method for three-dimensional seismic wave propagation. *Geophysical Journal International* **139**, 806-822, doi:10.1046/j.1365-246x.1999.00967.x (1999).
38 Komatitsch, D. & Vilotte, J.-P. The spectral element method: An efficient tool to simulate the seismic response of 2D and 3D geological structures. *Bulletin of the Seismological Society of America* **88**, 368-392 (1998).
39 Eberhart-Phillips, D. & Bannister, S. 3-D imaging of the northern Hikurangi subduction zone, New Zealand: variations in subducted sediment, slab fluids and slow slip. *Geophysical Journal International* **201**, 838-855, doi:10.1093/gji/ggv057 (2015).
40 Gutiérrez-Pastor, J., Nelson, C. H., Goldfinger, C. & Escutia, C. Sedimentology of seismo-turbidites off the Cascadia and northern California active tectonic continental margins, northwest Pacific Ocean. *Marine Geology* **336**, 99-119, doi:https://doi.org/10.1016/j.margeo.2012.11.010 (2013).
41 Van Daele, M. *et al.* A revised classification and terminology for stacked and amalgamated turbidites in environments dominated by (hemi)pelagic sedimentation. *Sedimentary Geology* **357**, 72-82, doi:10.1016/j.sedgeo.2017.06.007 (2017).
42 Talling, P. J., Masson, D. G., Sumner, E. J. & Malgesini, G. Subaqueous sediment density flows: Depositional processes and deposit types. *Sedimentology* **59**, 1937-2003, doi:10.1111/j.1365-3091.2012.01353.x (2012).

43 Barnes, P. M. & Audru, J. C. Quaternary faulting in the offshore Flaxbourne and Wairarapa Basins, southern Cook Strait, New Zealand. *New Zealand Journal of Geology and Geophysics* **42**, 349-367, doi:10.1080/00288306.1999.9514851 (1999).
44 Adams, J. Paleoseismicity of the Cascadia Subduction Zone: Evidence from turbidites off the Oregon-Washington Margin. *Tectonics* **9**, 569-583, doi:10.1029/TC009i004p00569 (1990).
45 Gutierrez-Pastor, J., Nelson, C. H., Goldfinger, C. & Escutia, C. Sedimentology of seismo-turbidites off the Cascadia and northern California active tectonic continental margins, northwest Pacific Ocean. *Marine Geology* **336**, 99-119, doi:10.1016/j.margeo.2012.11.010 (2013).
46 Ho, V. L., Dorrell, R. M., Keevil, G. M., Burns, A. D. & McCaffrey, W. D. Pulse propagation in turbidity currents. *Sedimentology* **65**, 620-637, doi:doi:10.1111/sed.12397 (2018).
47 Howarth, J. D., Fitzsimons, S. J., Norris, R. J., Langridge, R. & Vandergoes, M. J. A 2000 yr rupture history for the Alpine fault derived from Lake Ellery, South Island, New Zealand. *Bulletin of the Geological Society of America* **128**, 627-643, doi:10.1130/B31300.1 (2016).
48 Pouderoux, H., Proust, J. N. & Lamarche, G. Submarine paleoseismology of the northern Hikurangi subduction margin of New Zealand as deduced from Turbidite record since 16 ka. *Quaternary Science Reviews* **84**, 116-131, doi:10.1016/j.quascirev.2013.11.015 (2014).
49 Clark, K. *et al.* Geological evidence for past large earthquakes and tsunamis along the Hikurangi subduction margin, New Zealand. *Marine Geology* **412**, 139-172, doi:https://doi.org/10.1016/j.margeo.2019.03.004 (2019).
50 Bradley, B. A. *et al.* Ground motion simulations of great earthquakes on the Alpine Fault: effect of hypocentre location and comparison with empirical modelling. *New Zealand Journal of Geology and Geophysics* **60**, 188-198, doi:10.1080/00288306.2017.1297313 (2017).
51 Kearse, J., Kaneko, Y., Little, T. & Van Dissen, R. Curved slickenlines preserve direction of rupture propagation. *Geology* **47**, 838-842, doi:10.1130/g46563.1 (2019).
52 Townend, J. *et al.* Late-interseismic state of a continental plate-bounding fault: Petrophysical results from DFDP-1 wireline logging and core analysis, Alpine Fault, New Zealand. *Geochemistry, Geophysics, Geosystems* **14**, 3801-3820, doi:10.1002/ggge.20236 (2013).
53 Irikura, K. & Miyake, H. Recipe for Predicting Strong Ground Motion from Crustal Earthquake Scenarios. *Pure and Applied Geophysics* **168**, 85-104, doi:10.1007/s00024-010-0150-9 (2011).
54 Usami, K., Ikehara, K., Kanamatsu, T. & McHugh, C. M. Supercycle in great earthquake recurrence along the Japan Trench over the last 4000 years. *Geoscience Letters* **5**, doi:10.1186/s40562-018-0110-2 (2018).

Supplementary Information

Age of the turbidite

Multiple lines of evidence support very recent emplacement of the turbidites that we infer were formed in response to the Kaikōura earthquake. Excess ^{234}Th was measured in cores TAN1613-53 from the Hikurangi Trough (Fig. 1). Activities of 100-150 Bq.kg^{-1} of excess ^{234}Th were present in turbidite sediments, while the highest level of excess ^{234}Th activity of 480 Bq.kg^{-1} was detected in the oxic layer immediately beneath the turbidite[34] (Extended Data Fig. 1A). High levels of excess ^{234}Th activity in the turbidite sediment and the underlying oxidized layer provide unequivocal evidence of recent emplacement. At the time of coring (4 days after the Kaikōura earthquake) turbidites were highly fluidized, suggesting the deposit was still settling[34]. Additionally, fresh biological remains were identified in turbidite sediments from the Hikurangi channel, lending further support for deposition immediately prior to coring[34].

Sedimentary structures that support emplacement of new turbidites include burial of the reddish brown oxic layers underlying the deposits, at locations where the turbidity current has not eroded the seafloor. These oxic layers are characteristic of an un-disturbed seafloor where sediments have been at the sediment-water interface and subject to biological activity for extended periods. Oxic layers occur at the sediment water interface in pre-Kaikōura earthquake cores but are absent from the sediment water interface of Kaikōura turbidites (Extended Data Fig. 1C). The turbidites also exhibit no evidence of bioturbation, in contrast with the highly bioturbated underlying sediments (Extended Data Fig. 1A,B). The lack of bioturbation suggests insufficient time has elapsed following turbidite deposition to allow for colonisation and reworking of the sediments by benthic organisms. The utility of the degree of bioturbation as a proxy for recent deposition is provided by the quantifiable increase in bioturbation of the Kaikōura turbidite seen in cores TAN1613-53 and TAN1705-21 from the same Hikurangi Trough site but separated by 8 months between coring campaigns (Extended Data Fig. 1A,B). Despite these rapid bioturbation rates the Kaikōura deposit remains easily distinguishable and less bioturbated than the underlying pre-earthquake sea floor of older core top turbidites (Extended Data Fig. 1).

Evidence of the recent deposition of the 40 cm thick turbidite at site TAN1705-27, located in the axis of the Cook Straight Canyon, was also established by repeat coring. This site was first cored on 11 November 2016, several days before the Kaikōura earthquake and then again 8 months later on 5 May 2017. The absence of the 40 cm turbidite in the pre-earthquake core supports the Kaikōura earthquake origin of this bed.

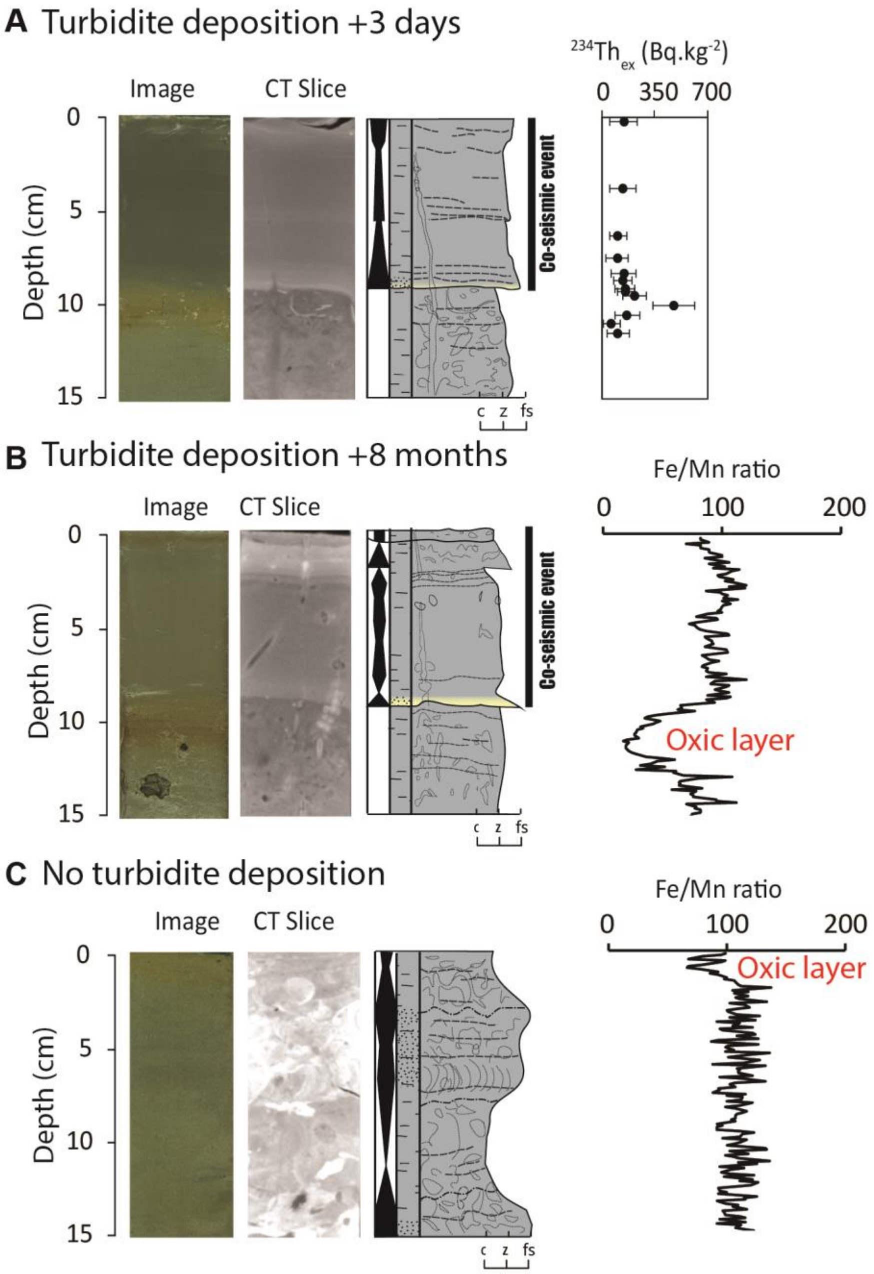

Extended Data Figure 1: Repeat coring at the Hikurangi Trough site. A) Core top turbidite in a core taken 3 days after the 2016 Kaikōura earthquake. The Kaikōura turbidite overlies an oxic pre-earthquake sea floor and excess ^{224}Th activity profiles confirm very recent deposition. B) Core top turbidite in a core taken 8 months after the Kaikōura earthquake. C) Highly bioturbated pre-Kaikoura core top turbidite with oxic layer developed at the sediment-water interface, as shown by the decrease in the Fe/Mn ratio from core site TAN1705-22. Quantifiable bioturbation of the Kaikōura event bed has occurred in the 8 months since deposition indicating that bioturbations rates are rapid.

Sediment Core Lithofacies.

The set of 23 cores provides insights into the presence/absence of deposits formed by Kaikōura earthquake triggered turbidity currents and informs the spatial extent of triggering in discrete canyons along the Hikurangi Subduction Margin (HSM).

Turbidites deposited by the Kaikōura earthquake range in thickness from 20–650 mm (Fig. 1A). The thickest turbidites associated with the Kaikōura earthquake occur in the thalweg of the Hikurangi Channel, >680 km north of the source area [34]. In the southern canyons the turbidites are all less than 50 mm thick (Fig. 2), while in the northern canyons they range from 20–400 mm thick (Fig. 2). Turbidite thickness in the northern canyons decreases from South to North along the margin (Fig. 2).

The stratigraphy of the turbidites deposited by Kaikōura earthquake turbidity currents varies in complexity between the southern and northern canyons (Extended Data Fig. 2A). In the southern canyon turbidites are characterised a ~5 mm thick basal lamination of very fine sandy silt (T_D) that is overlain by a normally graded, massive silty mud (T_{E-2}) that has a sharp, flat-lying lower contact (Extended Data Table 1). These T_D–T_{E-2} beds are interpreted to have formed by deposition from a waning turbidity current. Put another way, the turbidites are interpreted to have formed by a turbidity current surge with a single velocity pulse.

Kaikōura turbidites in the northern canyons have much more complex sedimentary structures. They are generally characterised by three stacked, normally graded bands (i.e. thicker than laminations but all within a single bed), each separated by sharp, sometimes loaded contacts (Extended Data Fig. 2B). Each normally graded band is characterised by 10–50 mm of planar laminated, very fine, sandy silt (T_D) that grades into 5–100 mm of planar laminated and normally graded mud (T_{E-1}) or massive and normally graded mud (T_{E-2}). Two exceptions occur within the northern canyons: (1) in core TAN1705 23 from the northernmost slope canyon, the coseismic turbidite is only 20 mm thick and has two fining upward sequences; and, (2) in core TAN1705 27 from the axis of the Cook Straight Canyon (the largest canyon system in the HSM), a 40 cm thick turbidite is much coarser (up to small pebbles) than the other silt-dominated turbidites described herein (Fig. 1). Despite the variation in texture, this Cook Strait Canyon turbidite is still comprised of three normally graded bands separated by sharp contacts (Fig. 2). The lower two sequences are composed of planar bedded, coarse to medium sand (T_{B-1}), overlain by cross-laminated, silty, fine sand that is rich in shell fragments (T_C). The uppermost, normally graded sequence has a basal band of planar bedded, medium to fine sand (T_{B-1}), separated from the overlying normally graded mud (T_{E-2}) by a sharp contact. The presence of low density shell-hash layers in the second T_C band obscures the relationship between density and grainsize observed in other cores. For example, the density trough at 200 mm on the TAN1705 27 core appears to be an artefact of the loosely consolidated shell hash rather than a reduction in grainsize. The lighter colouring in the core image through the T_C intervals is indicative of finer grainsizes compared to the underlying T_{B-1} interval. Hence, three normally graded bands can be clearly observed in the high-resolution core image. The stacked set of three normally graded bands in the majority of turbidites from the northern canyons is interpreted to be deposited by a surging turbidity current that had three distinct velocity pulses.

As noted above, cores that lack lithological evidence of a recently deposited turbidite have core tops characterised by heavy bioturbation and the presence of a reddish brown oxic layer at the sediment water interface (Extended Data Fig. 1C).

Extended Data Table 1: Description of core lithofacies from the canyons and slope basins cored in this study.

Lithofacies*	Description	Interpretation
T_{B-1}	Up to 100 mm thick beds of planar laminated coarse to medium sand.	Formed by reworking of coarse to medium sand grains as bedload beneath a low density turbidity current
T_C	Up to 100 mm thick beds of ripple cross-laminated, medium to fine sand.	Formed by reworking of medium to fine sand grains as bedload beneath a low density turbidity current.
T_D	Up to 50 mm thick beds of planar bedded, fine sand and very fine sandy silt.	Formed by reworking of very fine sand and coarse grains as bedload beneath a low density turbidity current.
T_{E-1} and T_{E-2}	Up to 100 mm thick, planar bedded, or normally graded mud.	Formed by settling from a low density turbidity current.

*Turbidite classification after Talling et al.[42].

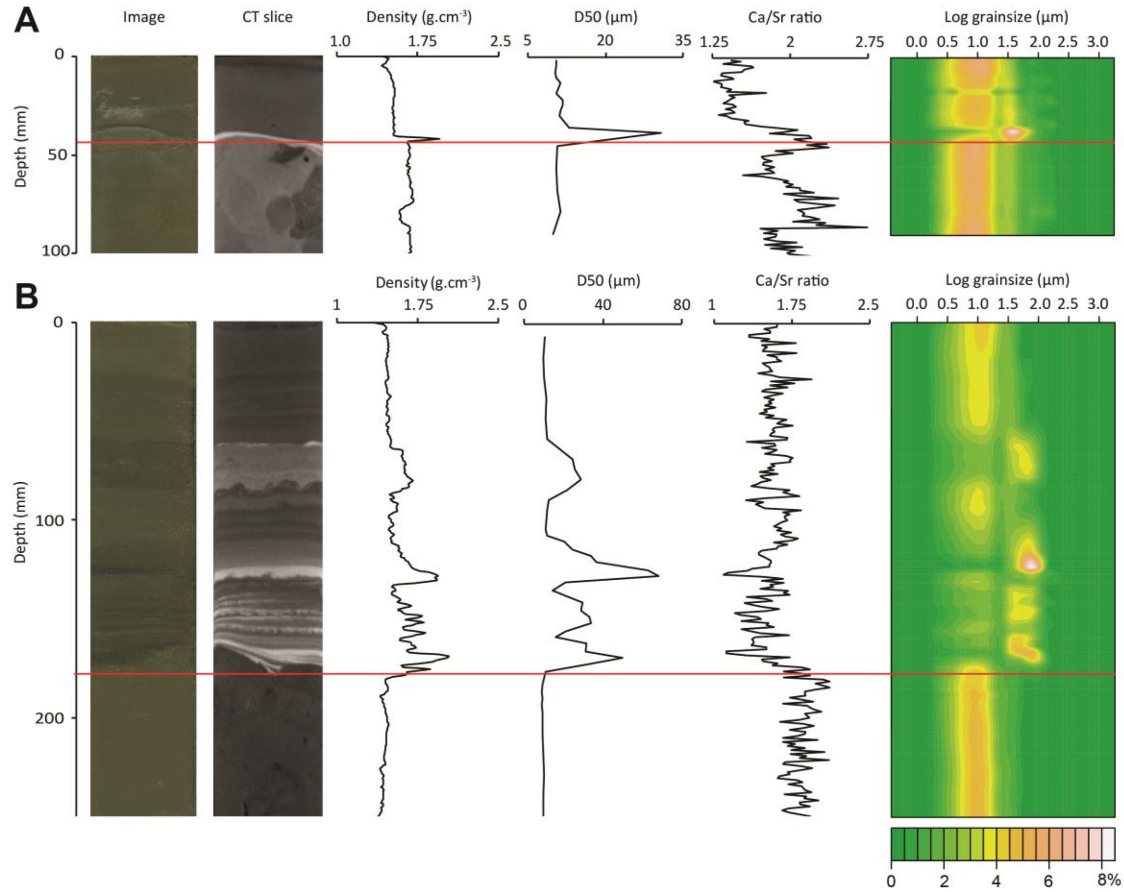

Extended Data Figure 2: The relationship between grainsize and bulk density derived from CT tomography. A) Linescan image, CT tomography sagittal slice, bulk density, grainsize D50, Ca/Sr ratio and grainsize heat map for TAN1705 36, a representative core for single-banded turbidite character from the southern canyons. B) Linescan image, CT tomography sagittal slice, bulk density, grainsize D50, Ca/Sr ratio and grainsize heat map for TAN1705 36, which is a representative core for tripartite-banded turbidite character from the northern canyons. Bulk density correlates very well with D50 in both simple and complexly bedded turbidites.

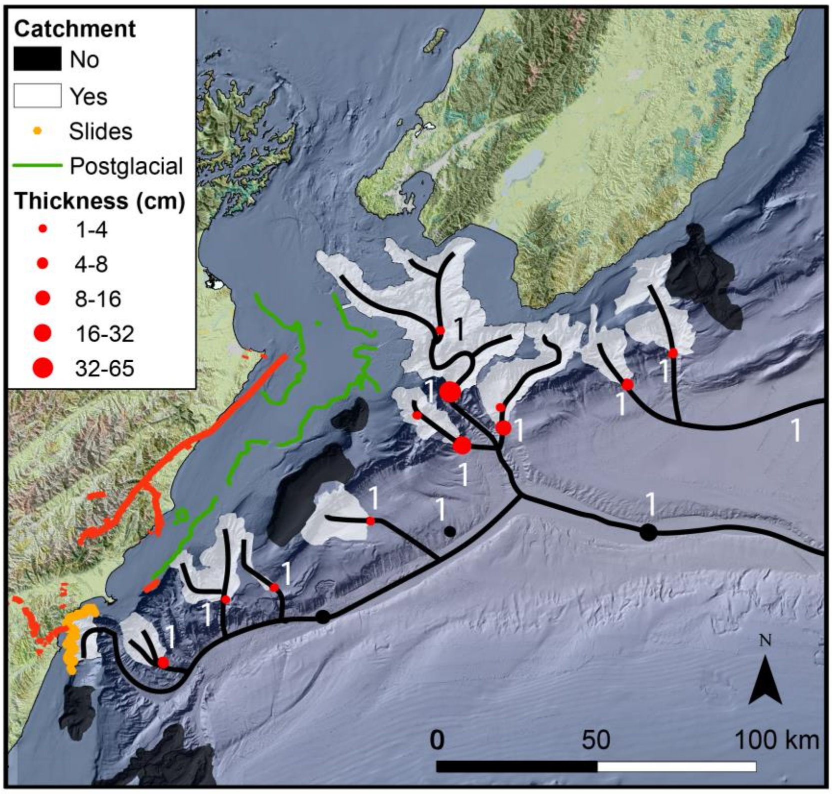

Extended Data Figure 3: Count of turbidites deposited by the Kaikōura earthquake up- and downstream of major channel and canyon confluences. A single turbidite was identified up- and downstream of all major flow path confluences, supporting the hypothesis underpinning the confluence test as a robust approach for establishing synchronous deposition of turbidites in the sedimentary record. Green lines represent the 0 m sediment isopach thickness for post-last glacial (<20 kyr) deposits within the Flaxbourne Basin on the eastern Marlborough continental shelf. The seaward edge of the basin deposit does not extend east to the shelf break, where there are structurally-uplifted mid Pleistocene or older units outcropping at the seafloor[43]. The consolidation state of the sediments in the head of the adjacent upper-slope gully may provide an explanation why no turbidity current was triggered there by the Kaikōura earthquake.

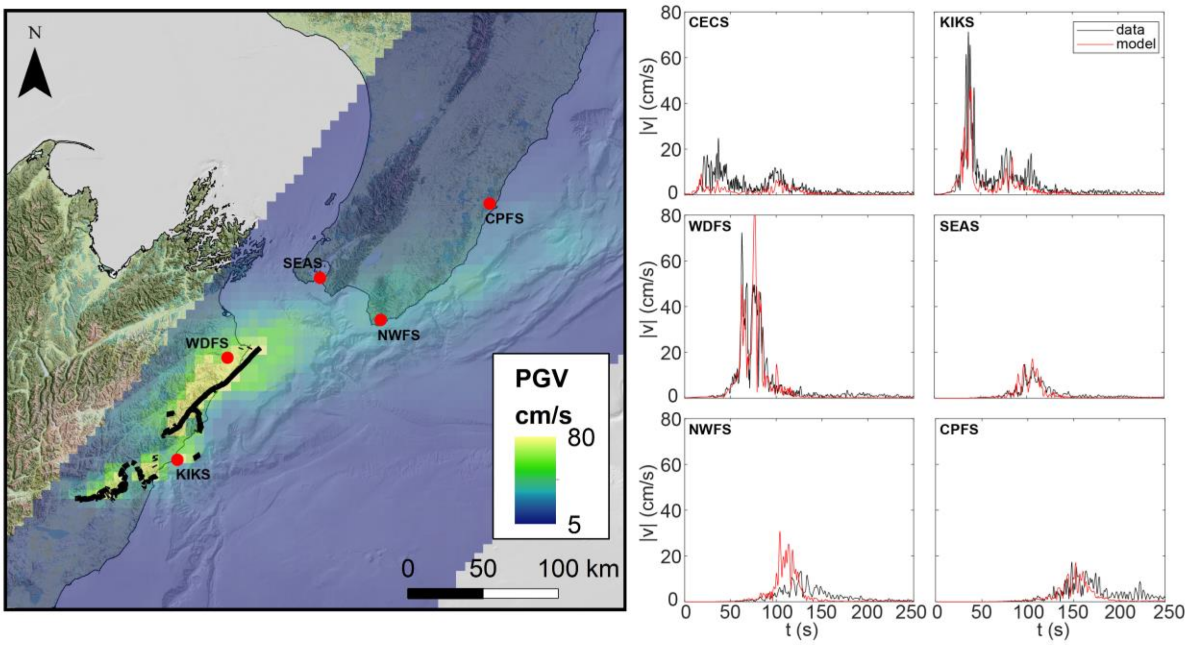

Extended Data Figure 4: Physics-based simulation of strong ground motions generated by the Kaikōura earthquake. Peak Ground Velocity (PGV) is shown along the southern Hikurangi Margin (A). The model shows excellent agreement with measured velocity time histories from seismic stations located along the length of the margin (B).

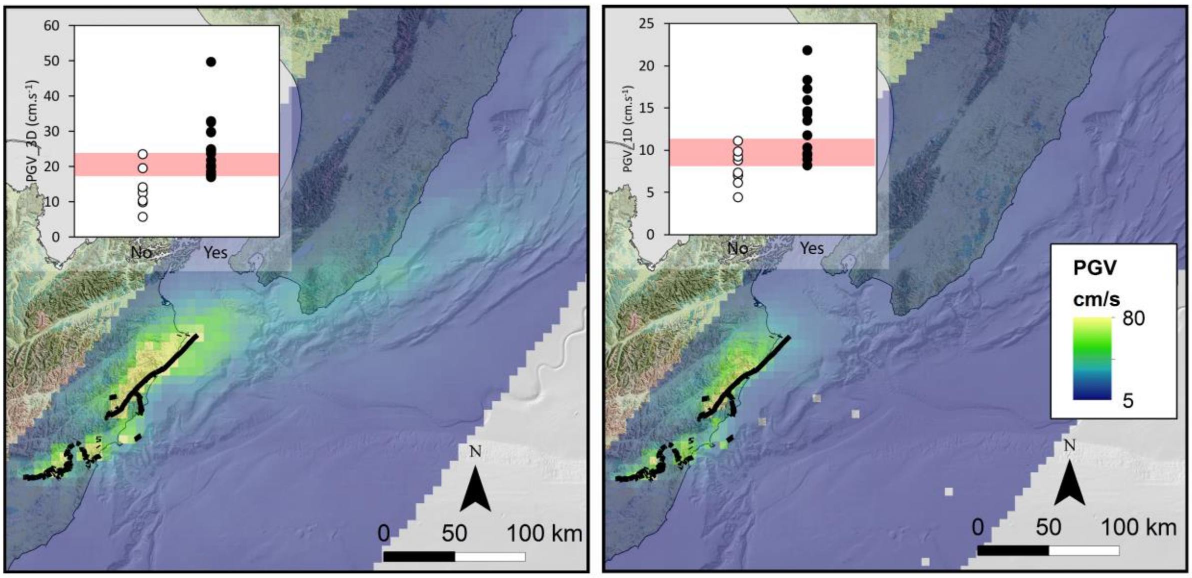

Extended Data Figure 5: **Comparison of simulated peak ground velocities for the Kaikōura earthquake.** The simulations are produced with (A) the 3D velocity model and (B) the 1D, layered velocity model.

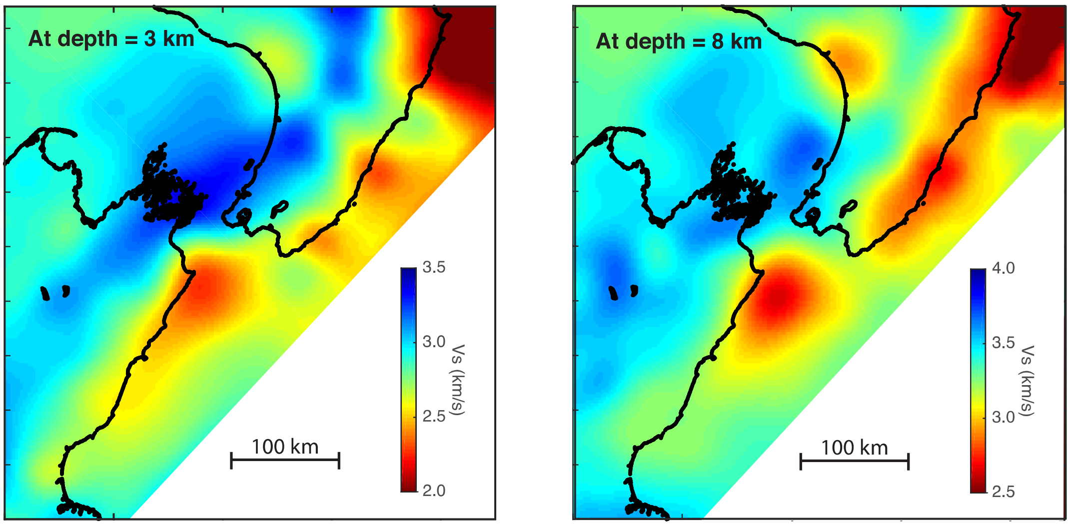

Extended Data Figure 6: Map of shear-wave velocity (Vs) at 3-km and 8-km depths in the velocity model. The offshore velocity is constrained by onshore-offshore data from marine air-gun shots recorded at onshore station[39].